Fixed Switching Frequency Model Predictive Control and Passivity Based Control for DC-DC Converter

Yajing Zhang[1*],Yuqing Shen[1],BaoYing Huang[2],Jiangchao Zhang[2],

and Haojing Chang[3]

[1] School of Automation, Beijing Information Science & Technology University, Beijing
[2] State Grid Economic and Technological Research Institute Co., Ltd, Beijing
[3] State Grid Corporation Gansu Power Grid Construction Division, Gansu

Abstract. The DC-DC converter represents a crucial component in the renewable energy sources. The stability and dynamic capability enhancement of the DC/DC converter have emerged as a significant research topic in the current era. Model predictive control (MPC) is particularly prevalent due to its high dynamic response speed, simplicity of the controller design, and capacity for multi-objective optimization. However, the traditional finite control set model predictive control (FCS-MPC) method is suffer to variable switching frequency and vast computing. To improve the dynamic performance of the converter, a novel nonlinear control strategy named fixed switching frequency MPC and passivity-based control (PBC), named FSF-PBMPC, is proposed, which could achieve fixed switching frequency and enhance the system's dynamic response speed. Firstly, the Euler-Lagrange (EL) model of the boost converter is established. Secondly, the relationship between duty cycle and MPC is established. Ultimately, the output voltage of PBC is incorporated into the cost function of the FCS-MPC. The characteristics of PBC power shaping and damping injection can enhance the system's immunity to interference, improve the system's dynamic response speed, and thus reinforce the system's stability. Then, depending on MATLAB, the simulation results proved that the proposed strategy has the same effect as we expected.

Key words: DC-DC Converter; FCS-MPC; Passivity-Based Control

1. INTRODUCTION

The growing interest in distributed generation technology has been driven by the emergence of energy scarcity and energy security concerns. As the increasing integration of renewable energy sources, such as photovoltaic and wind power generation, connected to distributed power generation systems, the randomness and volatility of the renewable sources, including enhancing dynamic performance, steady state characteristics, and full load range characteristics of the converter [1-2]. The DC-DC converter plays an important role as an interface for distributed power generation into the grid, as shown in Fig.1. Fig.1 illustrates the configuration of a classical DC microgrid, comprising photovoltaic power generation module, battery module, DC and AC loads. The DC bus voltage level, serves as the power processing unit for new energy generation in the microgrid through a converter.
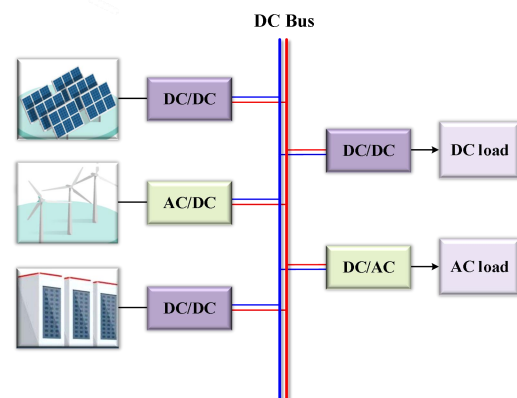
Fig.1 Schematic diagram of DC microgrid

The nonlinear characteristics of the distributed power generation system, as previously highlighted, present challenges to the traditional linear controllers [3]. The response speed of the control method and the stability of the controlled variables are particularly important for the system. The regulation goal of the DC-DC converter is to reach a stable value of the output voltage. Researchers have proposed

a variety of control methods to address the difficulty of regulating the output voltage to a stable value [4-5]. To better characterize the nonlinear characteristics of systems and improve their dynamic performance, nonlinear control has received widespread attention [6-9]. For example, sliding mode control [10-11], fuzzy control [12], internal model control [13], feedback linearization control [14]. Among the aforementioned control strategies, the traditional sliding mode control exhibits high robustness [15]. However, the design of the control signal is more intricate. The utilization of fuzzy control demonstrates improved regulation of the converter with enhanced nonlinear characteristics, as evidenced in the literature [16]. However, the limitation of the fuzzy rule design makes the method require re-designing of the rules under varying operating conditions, resulting in an increased number of fuzzy rules and subsequent computational complexity. Literature [17] devised an IDA-PBC with complementary PI controllers, which eradicates the steady-state error through the implementation of complementary PI controllers. This method offers a rapid dynamic response speed, robust immunity to interference, and high stability. However, its response speed to external disturbances is relatively slow. In response, literature [18] has proposed a PI-PBC method and utilized a parameter estimation-based observer to estimate the converter inductor current. In recent years, MPC has gained prominence as a prominent control strategy in the electrical field [19], which has advantages in dynamic response speed, immunity and implementation. MPC could be categorized into two distinct groups, including FCS-MPC and continuous control set model predictive control (CCS-MPC) [20-21]. Initially, the FCS-MPC controller has been widely employed in converters because of its simple design, ability to achieve multi-objective optimization, and fast dynamic response [22-25]. However, the traditional FCS-MPC strategy produces variable switching frequency during the control process, which will result in the saturation of boundaries in the inductor circuit ripple, and present a challenge in the design of the filter. Furthermore, fluctuations in the switching frequency may also result in increased energy consumption and a reduction in system efficiency. To tackle this problem, a solution for achieving the fixed switching frequency is raised in [26]. The fixed switching frequency MPC is employed in literature [27], which achieves the control of the fixed switching frequency by adjusting the inductor current ripple variation in the cost function. Nevertheless, the switching frequency continues to fluctuate due to alterations in system parameters.

To address the aforementioned issues, a nonlinear control method that integrates passive theory and fixed switching frequency MPC named FSF-PBMPC is proposed in this paper. Firstly, the Euler-Lagrange model of the Boost converter is established. Secondly, MPC exports the duty cycle signal. Finally, the PBC output voltage is incorporated into the cost function of the FCS-MPC with fixed switching frequency. The system's dynamic response speed is enhanced by eliminating the necessity for additional control loops, while its immunity to external parameter changes is also improved. This paper

uses the Boost converter as a model, and the simulation results verify the validity of the method.

This paper's organizations are shown as follows. In section II, the mathematical model of the Boost converter is presented. In section III, the model of the FSF-PBMPC is proposed, it introduces PBC output voltage to the MPC with a fixed switching frequency. In section IV, the simulation results are analyzed. Finally, the conclusions of this strategy are analyzed in section V.

2. MATHEMATICAL MODEL OF THE BOOST CONVERTER
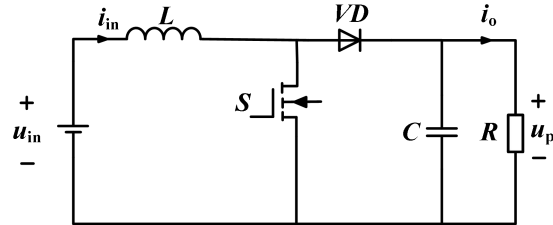
Fig.2. The Boost converter with resistive load

The Boost converter can be shown as an example to expand the modeling analysis of the proposed strategy, for the reason that it represents the typical converter. As in Fig. 2, the topology of a Boost converter is represented, where L is the inductor inductance, C is the capacitor, R represents the load, S represents the main switch, VD is the diode. Here, i_{in} is the inductor current, u_{in} is the input voltage, and u_p is the output voltage.

Based on the theory of Kirchhoff, we can get the state-space model of the Boost converter in the continuous-time domain which is the Eq. (1).

$$\begin{cases} L\dfrac{di_{in}}{dt} = u_{in} - (1-s)\cdot u_p \\ C\dfrac{du_p}{dt} = (1-s)\cdot i_{in} - \dfrac{u_p}{R} \end{cases} \tag{1}$$

3. IMPLEMENTATION OF THR PROPOSED FSF-PBMPC CONTROLLER

3.1. PBC Based Nonlinear Design of the Boost Converter.

Before applying the nonlinear control strategy to the central converter, the PBC model of the system should be given first. Initially, the Eq. (1) could be expressed as

$$A\frac{dx}{dt} + Bx + Rx = U \tag{2}$$

Where $A = \begin{bmatrix} L & 0 \\ 0 & C \end{bmatrix}$, $B = \begin{bmatrix} 0 & 1-s \\ s-1 & 0 \end{bmatrix}$, $R = \begin{bmatrix} 0 & 0 \\ 0 & \dfrac{1}{R} \end{bmatrix}$,

$U = \begin{bmatrix} u_{in} \\ 0 \end{bmatrix}$, $x = \begin{bmatrix} x_1 & x_2 \end{bmatrix}^T = \begin{bmatrix} i_{in} & u_p \end{bmatrix}^T$, $\dot{x} = \begin{bmatrix} \dfrac{dx_1}{dt} & \dfrac{dx_2}{dt} \end{bmatrix}^T$

The desired state space expression is $\boldsymbol{x}^* = \begin{bmatrix} x_1^* & x_2^* \end{bmatrix}^T = \begin{bmatrix} i_{\text{in}}^* & u_{\text{p}}^* \end{bmatrix}^T$, where i_{in}^* and u_{p}^* represent the inductor's desired current and desired output voltage, respectively. The PBC ultimately results in the state variable x reaching a value of x^*. The state vector error is set as $\boldsymbol{e} = x - x^*$.

Usually, the EL model based on the PBC theory could be expressed as

$$A\frac{\mathrm{d}\boldsymbol{e}}{\mathrm{d}t} + R\boldsymbol{e} = U - (A\frac{\mathrm{d}\boldsymbol{x}^*}{\mathrm{d}t} + Bx + Rx^*) \qquad (3)$$

Where $\dfrac{\mathrm{d}\boldsymbol{e}}{\mathrm{d}t}$ denotes the derivative of the error, $\dfrac{\mathrm{d}\boldsymbol{x}^*}{\mathrm{d}t}$ represents the derivative of x^*, and the error function of the system is

$$H_e(x) = \frac{1}{2}e^T A e \qquad (4)$$

In order to let the error energy storage function converge to zero with the greatest possible speed, it is necessary to inject damping into the system. The injected damping can be expressed as R_{p}.

$$R_a e = (R_p + R)e \qquad (5)$$

Where, $\boldsymbol{R}_p = \begin{bmatrix} R_{1p} & 0 \\ 0 & \dfrac{1}{R_{2p}} \end{bmatrix}$, $R_{1p} > 0$, $R_{2p} > 0$.

By substituting $e = x - x^*$ into Eq. (2) and the damping matrix is added to both sides of the equation, the error model of the Euler-Lagrange (EL) could be expressed as [28].

$$A\frac{\mathrm{d}\boldsymbol{e}}{\mathrm{d}t} + R\boldsymbol{e} + R_p\boldsymbol{e} = U - (A\frac{\mathrm{d}\boldsymbol{x}^*}{\mathrm{d}t} + Bx + Rx^*) + R_p\boldsymbol{e} \qquad (6)$$

Further, the controller of PBC could be denoted as follow

$$U = A\frac{\mathrm{d}\boldsymbol{x}^*}{\mathrm{d}t} + Bx + Rx - R_p\boldsymbol{e} \qquad (7)$$

3.2. Fixed Switching Frequency MPC Based Nonlinear Design of the Boost Converter.

If the sampling frequency in Eq. (1) is sufficiently high, using the Euler discretization method to discretize it, leading to the following equation

$$\begin{cases} u_{\text{p}}(m+1) = u_{\text{p}}(k) + \dfrac{T_s}{C}[i_L(m)(1-s) - \dfrac{u_{\text{p}}(m)}{R}] \\ i_{\text{in}}(m+1) = i_{in}(m) + \dfrac{T_s}{L}u_{\text{in}} - \dfrac{T_s}{L}u_{\text{p}}(m)(1-s) \end{cases} \qquad (8)$$

According to the Eq. (8), the i_{in} and u_{p} at the moment $m+1$ can be predicted, m represents the current moment. Meanwhile, the discrete sampling time is T_s.

The objective of MPC is typically to ensure that the converter provides a stable output voltage to the load. The most direct method for controlling the output voltage is to employ the cost function, which is followed by the direct inductor current MPC, and based on the aforementioned cost

function. Subsequently, the cost function for MPC is constructed.

$$\begin{cases} J_1 = \displaystyle\sum_{k=1}^{N} (i_{\text{in}}^*(m) - i_{\text{in}}(m+1))^2 \\ J_2 = \displaystyle\sum_{k=1}^{N} (u_{\text{p}}^*(m) - u_{\text{p}}(m+1))^2 \end{cases} \qquad (9)$$

Then, this paper proposes a further enhancement by re-modifying the differential equation of the i_{in}. It is achieved by ensuring that the input power is tantamount to the output power, which is obtained as

$$i_{\text{in}} = \frac{u_{\text{p}} i_{\text{o}}}{u_{\text{in}}} \qquad (10)$$

Where, i_{o} is the system's output current, and then substitute it to the Eq. (8), Eq. (11) is obtained as

$$\begin{cases} u_{\text{p}}(m+1) = u_{\text{p}}(k) + \dfrac{T_s}{C}[i_{\text{in}}(m)(1-s) - \dfrac{u_{\text{p}}(m)}{R}] \\ i_{\text{in}}(m+1) = i_{\text{in}}(m) + \dfrac{T_s}{L}u_{\text{in}} - \dfrac{T_s}{L}\sqrt{i_{\text{in}}(m)u_{\text{in}}R}(1-s) \end{cases} \qquad (11)$$

Substituting the $u_{\text{p}}(m+1)$, $i_{\text{in}}(m+1)$ calculated in Eq. (11) into the Eq. (9) to obtain the cost function for single-step optimization MPC is expressed as

$$J = (i_{\text{in}}(m) - \frac{(1-s)}{L}\sqrt{i_{\text{in}}(m)u_{\text{in}}RT_s} + \frac{1}{L}u_{\text{in}}T_s - i_n^*)^2$$
$$+ (u_{\text{p}}(m) + \frac{(1-s)}{C}i_{\text{in}}(m)T_s - \frac{1}{RC}u_{\text{p}}(m)T_s - u_{\text{p}}^*)^2 \qquad (12)$$

In order to get the control signal, this paper establishes a direct correlation between the duty cycle and the MPC.

$$\frac{\partial J}{\partial s} = \frac{\partial[(i_{\text{in}}(m+1) - i_n^*)^2 + (u_{\text{p}}(m+1) - u_{\text{p}}^*)^2]}{\partial s} = 0 \qquad (13)$$

By the tenets of Eq. (13), the Eq. (4) is obtained

$$D = \frac{(i_{\text{in}}(m) - \frac{1}{L}\sqrt{i_{\text{in}}(m)u_{\text{in}}RT_s} + \frac{1}{L}u_{\text{in}}T_s - i_n^*)\frac{1}{L}\sqrt{i_{\text{in}}(m)u_{\text{in}}RT_s}}{-\frac{1}{C^2}i_{\text{in}}(m)^2T_s^2 - \frac{1}{L^2}i_{\text{in}}(m)u_{\text{in}}RT_s^2}$$
$$-\frac{(u_{\text{p}}(m) + \frac{1}{C}i_{\text{in}}(m)T_s - \frac{1}{RC}u_{\text{p}}(m)T_s - u_{\text{p}}^*)\frac{1}{C}i_{\text{in}}(m)T}{-\frac{1}{C^2}i_{\text{in}}(m)^2T_s^2 - \frac{1}{L^2}i_{\text{in}}(m)u_{\text{in}}RT_s^2} \qquad (14)$$

In this scenario, the cost function will attain its minimal value upon the adoption of the optimally derived variable D.

3.3. The proposed FSF-PBMPC nonlinear design for the Boost converter.

To further accelerate the system's response speed and reduce the computational complexity of MPC, this paper aims to combine the PBC and the fixed switching frequency MPC, named fixed switching frequency MPC based on passivity-

based control. The model based on the proposed control strategy could be expanded as

$$\begin{cases} u_{in} = L\dfrac{di_{in}^*}{dt} + (1-s)u_p - R_{1p}(i_{in} - i_{in}^*) \\ 0 = C\dfrac{du_p^*}{dt} - (s-1)i_{in} + \dfrac{1}{R}u_p^* - \dfrac{1}{R_{2p}}(u_p - u_p^*) \end{cases} \quad (15)$$

Equation (15) represents the PBC equation. Furthermore, i_{in}^* and u_p^* are the reference values of the i_{in} and u_p, respectively. Thus, $\dfrac{di_{in}^*}{dt} = 0$, $\dfrac{du_p^*}{dt} = 0$. Therefore, the electrical subsystem can be described as:

$$\begin{cases} i_{in}(m) = \dfrac{1}{R_{1p}}[(1-s)u_p(m) - u_{in}(m)] + i_{in}^*(m) \\ u_p(m) = R_{2p}[(s-1)i_{in}(m) + \dfrac{1}{R}u_p^*(m)] + u_p^*(m) \end{cases} \quad (16)$$

From this, it can be concluded that

$$u_p(m) = \dfrac{u_{in}i_{in}^*R}{u_p^*} + \dfrac{R_{1p}i_{in}^*R(i_{in}^* - i_{in})}{u_p^*} \quad (17)$$

Substituting of Eq. (17) into Eq. (14), then the final control expression is

$$D = \dfrac{(i_{in}(m) - \frac{1}{L}\sqrt{i_{in}(m)u_{in}RT_s} + \frac{1}{L}u_{in}T_s - i_{in}^*)\frac{1}{L}\sqrt{i_{in}(m)u_{in}RT_s}}{-\frac{1}{C^2}i_{in}(m)^2T_s^2 - \frac{1}{L^2}i_{in}(m)u_{in}RT_s^2}$$
$$-\dfrac{(u_p(m) + \frac{1}{C}i_{in}(m)T_s - \frac{1}{RC}u_p(m)T_s - u_p^*)\frac{1}{C}i_{in}(m)T_s}{-\frac{1}{C^2}i_{in}(m)^2T_s^2 - \frac{1}{L^2}i_{in}(m)u_{in}RT_s^2} \quad (18)$$

Figure 3 illustrates the control block of the proposed control strategy for the Boost converter.
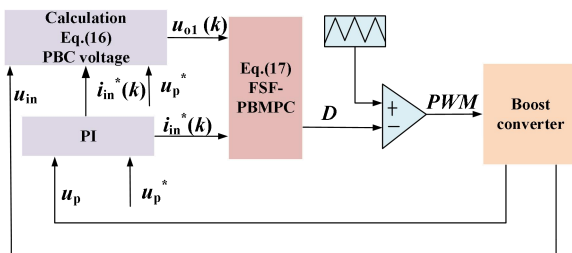
Fig.3. The control block of the proposed control strategy

3.4. Stability analysis of the proposed method

Since it is difficult to obtain the analytical form of the control loop transfer function for MPC, it leads to the difficulty of the traditional stability analysis methods. In

light of the fact that the Lyapunov function does not necessitate the availability of a transfer function, this paper employs it as a foundation for the proof of stability of the proposed control method.

The positive Lyapunov functions is denoted as

$$C = 0.5\,\|\,i_{in}^* - i_{in}(m)\,\|_2^2 \quad (19)$$

As shown in Eq. (19), this function is the Euclidean distance between the desired inductor current and the actual current. In this context, the Lyapunov function is represented by the symbol C.

Equation (19) is derived as follows:

$$\dot{C} = -\dfrac{di_{in}(k)^T}{dt} \cdot (i_{in}^* - i_{in}(m)) \quad (20)$$

With the model of the Boost converter, the Eq. (20) can be modified as

$$\dot{C} = -\dfrac{u_{in} - (1-s)u_p}{L} \cdot (i_{in}^* - i_{in}(m)) \quad (21)$$

Substituting Eq. (17) into Eq. (21), the following result is obtained:

$$\dot{C} = -\dfrac{u_{in} - (1-s)\dfrac{u_{in}i_{in}^*R}{u_p^*} + \dfrac{R_{1p}(i_{in}^* - i_{in}(m))}{u_p^*}}{L} \cdot (i_{in}^* - i_{in}(m))$$
$$-\dfrac{di_{in}^*(k)^T}{dt}(i_{in}^* - i_{in}(m)) \quad (22)$$

Where, $\dfrac{di_c^*(k)^T}{dt} = 0$. When $s = 0$, the Eq. (22) is a negative definite, indicating that the system is stable. When s = 1, the Eq. (22) is shown as

$$\dot{C} = -\dfrac{u_{in}u_p^* - R_{1p}(i_{in}^* - i_{in}(m))}{u_p^*L} \cdot (i_{in}^* - i_{in}(m)) \quad (23)$$

Substituting Eq. (16) into Eq. (23), Eq. (24) is obtained:

$$\dot{C} = -\dfrac{u_{in}u_p^* - \dfrac{u_{in}^2}{R_{1p}}}{u_p^*L} \quad (24)$$

Thus, it is established that the value is in fact negative, which consequently ensures the stability of the system.

To ensure that the system is stable, the injection damping R_{1p} is selected as 5Ω.

3.5. Selection of passive controller parameters

The passive controller injection damping R_{1P} variable is proportional to the stored energy of the inductor, whereas the R_{2P} variable depends on the stored energy of the capacitor. In order to ascertain the injection damping values, the inductor series resistance R_1 and the capacitor series resistance R_2 are employed in the following equivalent circuit state-space equations.

The state space equation of the equivalent circuit is shown as

$$\dot{x} = \begin{bmatrix} -\dfrac{R_1}{L} & -\dfrac{1-D}{L} \\ \dfrac{1-D}{C} & -\dfrac{1}{CR_2} - \dfrac{1}{CR} \end{bmatrix} x + \begin{bmatrix} \dfrac{1}{L} \\ 0 \end{bmatrix} u_{in} \qquad (25)$$

At this point the characteristic equation of Eq. (25) is

$$s^2 + (\frac{R_1}{L} + \frac{1}{CR_2} + \frac{1}{CR})s + \frac{(1-D)^2}{CL} + \frac{R_1}{CL}(\frac{1}{R_2} + \frac{1}{R}) = 0 \quad (26)$$

In order to relate R_1 and R_2 in the equivalent circuit to the damping injections R_{1p} and R_{2p}, Eq. (4) is simplified. It follows that:

$$A\dot{e} = -R_p e \qquad (27)$$

Simplifying through it gives as follows

$$\dot{x} = -\begin{bmatrix} \dfrac{R_{1p}}{L} & 0 \\ 0 & \dfrac{1}{CR_{2p}} \end{bmatrix} \begin{bmatrix} x_1 - x_1^* \\ x_2 - x_2^* \end{bmatrix} \qquad (28)$$

By associating Eq. (25) with Eq. (28), Eq. (29) can be get

$$\begin{cases} R_1 = \dfrac{u_{in} + R_{1p}i_{in} - R_{1p}i_{in}^* - (1-D)u_p}{i_{in}} \\ \dfrac{1}{R_2} = \dfrac{R}{CR_{1p}}(1 - \dfrac{u_p^*}{u_p}) + \dfrac{R}{Cu_p}(1-D)i_{in} - \dfrac{1}{C} \end{cases} \qquad (29)$$

At steady state u_{in}-$i_{in}R_{1p} = (1-D)u_p$, $i_{in}= i_{in}$*,we can get

$$\begin{cases} R_1 = R_{1p} \\ \dfrac{1}{R_2} = 0 \end{cases} \qquad (30)$$

Substituting Eq. (30) into Eq. (26) yields the equation characterizing the virtual equivalent circuit

$$s^2 + (\frac{R_{1p}}{L} + \frac{1}{CR})s + \frac{(1-D)^2}{CL} + \frac{R_{1p}}{CLR} = 0 \qquad (31)$$

At this point, the damping ratio ξ and R_{1p} of the system are respectively

$$\begin{cases} \xi = \dfrac{\dfrac{R_{1p}}{L} + \dfrac{1}{CR}}{2\sqrt{\dfrac{(1-D)}{CL} + \dfrac{R_{1p}}{CLR}}} \\ R_{1p} = \dfrac{(2\xi^2 - 1)L}{CR} + \sqrt{\left(\dfrac{2\xi^2 L - L}{CR}\right)^2 + \dfrac{4(1-D)\xi^2 L}{C}} \end{cases} \qquad (32)$$

The output voltage response of the closed-loop system under the action of the unit step signal is shown in Fig. 4 for damping ratios of 0.1, 0.5, 1, 1.5, and 2, respectively. It can be observed that when the damping ratio falls between 0 and 1, indicating an under damped state, the transient response of the system exhibits a sinusoidal oscillation curve with an amplitude that decays exponentially. In the case of $\zeta = 1$ or $\zeta >$ 1, the system is in the critical damping or over damping state, the transient response of the system presents a monotonically rising exponential curve, with no oscillation occurring. This indicates that the passive system is more stable. At this juncture, the value of R_{1p} should satisfy

$$R_{1p} \geq \frac{L}{CR} + \sqrt{\frac{L^2}{C^2R^2} + \frac{4(1-D)L}{C}} \qquad (33)$$

Combining the L and C parameters, $R_{1p} = 5\,\Omega$ is chosen in this paper.
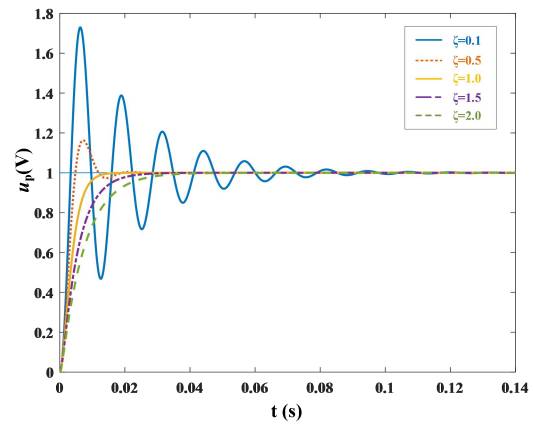
Fig. 4. Unit step response curve of the system

4. SIMULATION RESULTS

This paper employs the Boost converter as a case study for the verification of simulation results. Firstly, the fixed-switching frequency MPC is contrasted and analyzed with the non-fixed-switching frequency MPC. It is demonstrated that the interference immunity of the MPC is enhanced after fixing the switching frequency. Secondly, the simulation results are conducted for five cases, including inductance and capacitance change, sudden change of desired voltage, load, and input voltage. The simulation results demonstrate the efficacy of the proposed methodology. The parameters, which are employed in simulation presented in Table1. The calculation process of the proposed FSF-PBMPC is shown as Table 2.

TABLE 1. System simulation parameters

Parameter name	Symbol	Value	Unit
DC Input Voltage	u_{in}	50	V
Desired DC Output Voltage	u_p^*	100	V
Inductors	L	1.5	mH
Capacitors	C	1500	uF
Injection Damping	R_{1p}	5	Ω
Switching Frequency	f	20	kHz

Load Resistance	R	50	Ω
Proportionality	K_P	0.8	
Integral Adjustment	K_i	160	
Sampling Time	T_s	60	us

TABLE 2. System simulation parameters

Algorithm 1:FSF-PBMPC Algorithm

---

function FSF-PBMPC
1. Measure u_{in} , i_{in}
2. Collecting values of i_{in}^*
3. Setting the value of u_p^*
2. Calculate Eq. (17)
3. Calculate Eq. (18)
end
end function
Update D

According to the parameter values given in Table 1, we compare and analyze the proposed control method with fixed-switching frequency MPC in the Boost converter based on simulation results under varying input voltage, desired voltage, and load disturbance. Table 2 illustrates the calculation process of the implementation of the algorithm.

4.1. Comparative analysis of non-fixed-switching frequency MPC and fixed-switching frequency MPC.
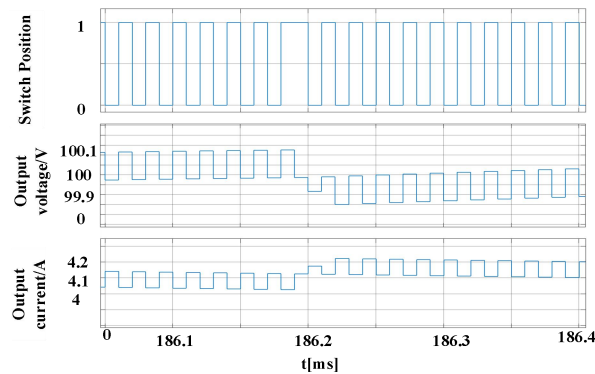
Fig.5. Non-fixed-switching frequency MPC
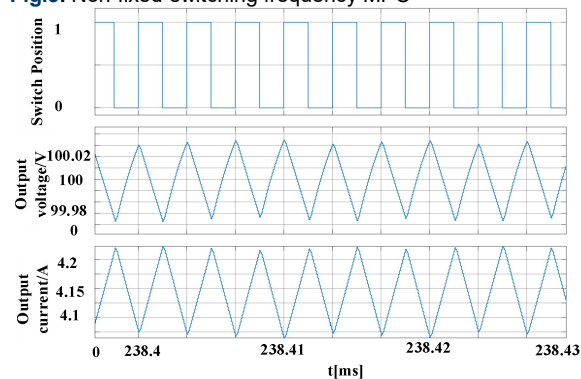
Fig.6. Fixed-switching frequency MPC

Figure 5 depicts the simulation results about the conventional MPC without fixed switching frequency. The variability of the controller can be observed. The controller's effect cannot be realized accurately, as indicated by the output voltage and output current ripple plots, it will result in a nonuniform about i_{in} and u_p.

Figure 6 displays the simulation results of the fixed switching frequency MPC, demonstrating the achieved outcomes of the fixed switching frequency MPC. The controller's effectiveness is accurately demonstrated by the output voltage's ripple diagrams and output current's ripple diagrams, resulting in a uniform inductor current and output voltage.

The results demonstrate that the stability of the system of the fixed-switching frequency MPC is enhanced. The controller's effectiveness is accurately demonstrated by the output voltage's ripple diagrams and output current's ripple diagrams.

4.2. Simulation of inductance and capacitance change.

The simulated waveform of the of the u_p and i_o of the Boost converter when the inductance and capacitance are performed as shown in Fig.7 and Fig.8.

Figure 7 shows the simulation results for the output voltage and output current as the inductance parameter is changed. To evaluate the effectiveness of the proposed control method, a graph of the control for the FSF-PBMPC was generated where the inductance parameter of the circuit was increased from its original value of 1mH to 2mH. After increasing the inductance, it was observed that the voltage and current fluctuations were minimal, as was the ripple fluctuation amplitude. Thus, the effect of the inductance parameter on the circuit was found to be insignificant, thus verifying the robustness of the method with respect to this parameter.
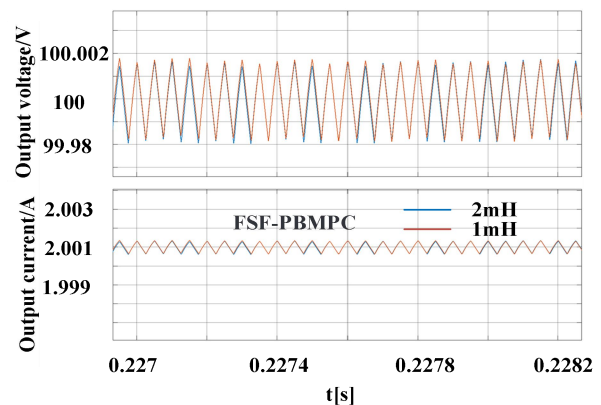
Fig.7. FSF-PBMPC Inductance increase comparison simulation results

Figure 8 illustrates the simulation result graph of the output voltage and output current after increasing the capacitance parameter. the capacitance parameter of the circuit is increased from 1500 µF to 2000 µF. Furthermore, an increase in capacitance resulted in a reduction in voltage and current fluctuations, as well as a decrease in ripple fluctuation amplitude. The impact on the circuit was also found to be minimal. Consequently, the robustness of this

method was verified in terms of the capacitance parameter. The impact on the circuit is minimal, thus verifying the robustness of the method in terms of capacitance parameters.
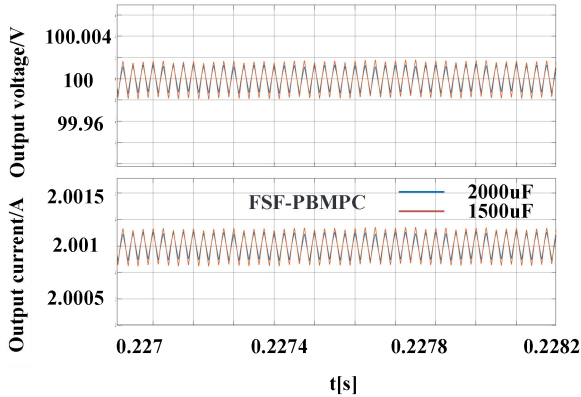
Fig.8. FSF-PBMPC capacitance increase comparison simulation results

4.3. Simulation of desired voltage change.

The simulated waveform of the of the u_p and i_o of the Boost converter when the desired voltage changes is performed as shown in Fig. 9. We compare the stabilization and response speed of these two control strategies under varying desired voltage conditions.

Figure 9 illustrates the waveforms of the u_p and i_o when the desired output voltage is altered. The initial voltage is set to 50V, the initial u_p^* is set to 70V, and the u_p^* is set to 100V at 0.3s. The addition of PBC accelerates the system's dynamic response, and the overshoot of the system is reduced.
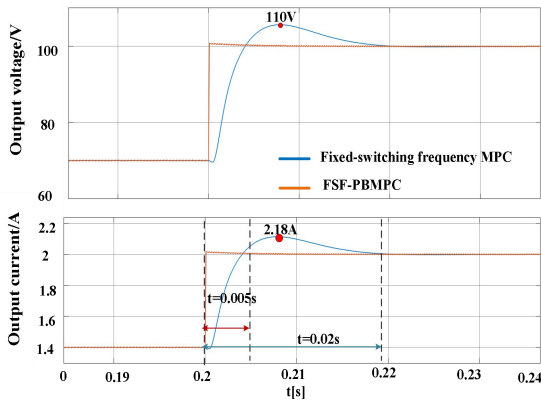
Fig.9. Comparison of desired voltage change simulation of fixed-frequency MPC and proposed control

4.4. Simulation of load disturbance change.

In Fig. 10, the waveforms of the u_p and i_o of the system when the load is varied. The initial voltage is 50V, and the u_p^* is 100V. The initial load is set to 50Ω, and a 50Ω resistor is connected in parallel at both ends of the load at 0.3s. The total resistance is 25Ω. As illustrated in the graph, the dynamic response of the proposed control is more rapid, and there is no overshooting in the process.
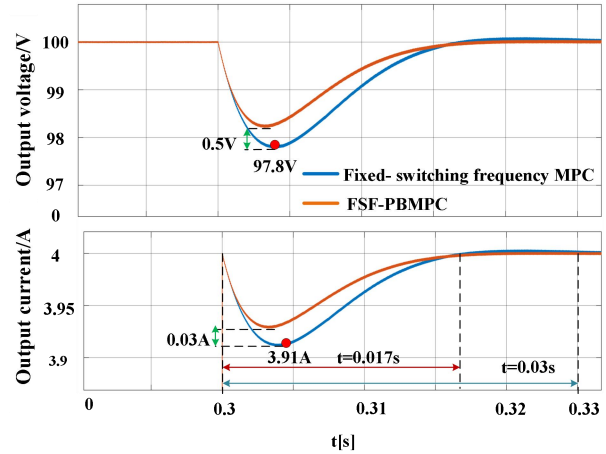
Fig.10. Comparison of load disturbance change simulation of fixed-frequency MPC and proposed control

4.5. Simulation of input voltage change.

As shown in Fig. 11, it illustrates the waveforms of the u_p and i_o when the u_{in} is varied. At begin, u_{in} is 50V, and the u_p^* is 100V. At 0.3s, u_{in} is varied from 50V to 60V. As illustrated in the figure, the overshoot is reduced and the dynamic response is accelerated for the proposed control.
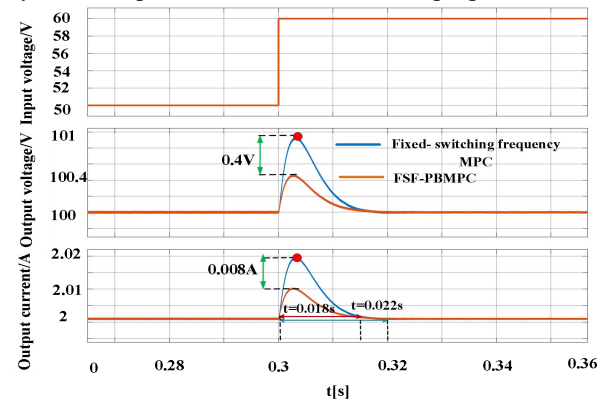
Fig.11. Comparison of input voltage change simulation of fixed-switching frequency MPC and proposed control

The simulation verification is conducted under five scenarios: inductance and capacitance change, sudden changes in the desired voltage, load, and the input voltage. The results indicate that the stability of the fixed switching frequency MPC is enhanced by the addition of PBC, while the dynamic response speed of the system is accelerated.

5. CONCLUSIONS

In this paper, a nonlinear control strategy named FSF-PBMPC is proposed, which is based on the FCS-MPC method and passive-based control theory. Firstly, the switching signals generated by the traditional model prediction are converted to the optimal duty cycle, thereby generating a fixed switching frequency. Secondly, passivity - based control is incorporated into the MPC framework to enhance the stability of the system and accelerate the system's response speed. The efficacy of the proposed method is validated through simulation based on MATLAB, leading to the following conclusions.

7

(1) The system's stability is improved under the proposed FSF-PBMPC control strategy with a fixed switching frequency. It is observed that the uniform inductor current and output voltage control effect is realized.

(2) Compared with the fixed-frequency MPC, the proposed FSF-PBMPC method enhances the system's anti-interference capability and improves the response speed by incorporating passive-based control. Furthermore, the proposed control strategy has faster dynamic response speed and no overshoot when the simulation conditions are varied.

(3) The proposed control strategy is capable of adapting to changes in operating conditions.

REFERENCES

[1] T. Dragičević, X. Lu, J. C. Vasquez and J. M. Guerrero, "DC Microgrids-Part I: A Review of Control Strategies and Stabilization Techniques," *IEEE Trans. Power Electron.*, vol. 31, no. 7, pp. 4876-489,2016, doi: 10.1109/TPEL.2015.2478859.

[2] Z. Karami, Q. Shafiee, S. Sahoo, M. Yaribeygi, H. Bevrani and T. Dragicevic, "Hybrid Model Predictive Control of DC–DC Boost Converters With Constant Power Load," *IEEE Trans. Energy Convers.*, vol. 36, no. 2, pp. 1347-1356, 2021, doi: 10.1109/TEC.2020.3047754.

[3] A. Reatti, F. Corti, A. Tesi, A. Torlai and M. K. Kazimierczuk, "Nonlinear Exact Analysis and Solution of Power Stage of DC-DC PWM Boost Converter," in *2019 IEEE Int. Symp. Circuits and Syst. (ISCAS)*, 2019, pp. 1-5, doi: 10.1109/ISCAS.2019.8702549.

[4] Z. Junzi, L. Ye, Y. Yuanyuan, H. Fuhua and Z. Xiaoqi, "A Novel Adaptive Control Strategy for Transient Performance Improvement of DC/DC Converter in Distributed Power Generation Systems," in *2022 IEEE/IAS Ind. and Commercial Power Syst. Asia (I&CPS Asia)*, 2022, pp. 570-576, doi: 10.1109/ICPSAsia55496.2022.9949908.

[5] P. Karamanakos, T. Geyer and S. Manias, "Direct Voltage Control of DC–DC Boost Converters Using Enumeration-Based Model Predictive Control," *IEEE Trans. Power Electron.*, vol. 29, no. 2, pp. 968-978, 2014, doi: 10.1109/TPEL.2013.2256370.

[6] L. Karunaratne, N. R. Chaudhuri, A. Yogarathnam and M. Yue, "Nonlinear Backstepping Control of Grid-Forming Converters in Presence of Grid-Following Converters and Synchronous Generators," *IEEE Trans. Power Syst.*, vol. 39, no. 1, pp. 1948-1964, 2024, doi: 10.1109/TPWRS.2023.3272528.

[7] J. H. Urrea-Quintero, N. Muñoz-Galeano and D. A. Cuervo-Sanchez, "A procedure for power electronic converters design with controllability verification based on the nonlinear dynamical model," in *2017 IEEE Workshop Power Electron. and Power Qual. Appl. (PEPQA)*, 2019, pp. 1-6, doi:10.18178/ijeee.5.3.207-212.

[8] F. Wang, G. Lin, and Y. He, "Passivity-Based Model Predictive Control of Three-Level Inverter-Fed Induction Motor," *IEEE Trans. Power Electron.*, vol. 36, no. 2, pp. 1984-1993, 2021, doi: 10.1109/TPEL.2020.3008915.

[9] L. Qiu, "Passivity-Based Cascade-Free Finite-Set Model Predictive Control for Nested Neutral Point-Clamped Converters," *IEEE Access*, vol. 8, pp. 200209-200218, 2020, doi: 10.1109/ACCESS.2020.3033272.

[10] Z. Yu, J. Zeng, J. Liu and F. Luo, "Terminal sliding mode control for dual active bridge dc-dc converter with structure of voltage and current double closed loop," in *2018 Australian & New Zealand Control Conf. (ANZCC)*, 2018, pp.11-15, doi:10.1109/ANZCC.2018.8606608.

[11] H. Sira-Ramirez, G. Escobar and R. Ortega, "On passivity-based sliding mode control of switched DC-to-DC power converters," in *Proc. of 35th IEEE Conf. Decision and Control*, 1996, pp. 2525-2526, doi:10.1109/CDC.1996.573474.

[12] F. Tlili and F. Bacha, "Fuzzy Logic Direct Power Control of a Bidirectional Three-Phase ACDC Converter," in *2020 20th Int. Conf. Sciences and Techn. Autom. Control and Comput. Eng. (STA)*, 2020, pp. 201-206, doi:10.1109/STA50679.2020.9329316.

[13] A. Ghosh and S. Banerjee, "A Comparison between Classical and Advanced Controllers for a Boost Converter," in *2018 IEEE Int. Conf. Power Electron., Drives and Energy Syst. (PEDES)*, 2018, pp. 1-6, doi:10.1109/PEDES.2018.8707911.

[14] J. Liu, W. Ming, and F. Gao, "A new control strategy for improving performance of boost DC/DC converter based on input-output feedback linearization," in *2010 8th World Congr. Intel. Control and Autom.*, 2010, pp. 2439–2444, doi:10.1109/WCICA.2010.5554675.

[15] B. Taheri and M. Sedaghat, "A new general controller for DC-DC converters based on SMC methods," in *2018 6th Int. Istanbul Smart Grids and Cities Congr. and Fair (ICSG)*, 2018, pp. 49-53, doi: 10.1109/SGCF.2018.8408940.

[16] N. Vafamand, S. Yousefizadeh, M. H. Khooban, J. D. Bendtsen and T. Dragičević, "Adaptive TS Fuzzy-Based MPC for DC Microgrids With Dynamic CPLs: Nonlinear Power Observer Approach," *IEEE Syst. J.*, vol. 13, no. 3, pp. 3203-3210, 2019, doi: 10.1109/JSYST.2018.2880135.

[17] J. Zeng, Z. Zhang and W. Qiao, "An Interconnection and Damping Assignment Passivity-Based Controller for a DC–DC Boost Converter With a Constant Power Load," *IEEE Trans. Ind. Appl.*, vol. 50, no. 4, pp. 2314-2322, 2014, doi: 10.1109/TIA.2013.2290872.

[18] L. Gupta, S. Bhandari, and Deepika, "Modelling of Passivity based Controller for Buck Boost Converter," in *2022 2nd Int. Conf. Next Gener. Intell. Syst. (ICNGIS)*, 2022, pp. 1-6, doi: 10.1109/ICNGIS54955.2022.10079798.

[19] W. Ao and J. Chen, "Model Predictive Control of Four-Switch Buck-Boost Converter for Pulse Power Loads," in *2021 IEEE Int. Conf. Predictive Control Elect. Drives and Power Electron. (PRECEDE)*, 2021, pp. 904-908, doi: 10.1109/PRECEDE51386.2021.9680981.

[20] S. Ni, Z. Zheng, L. Peng and Y. Li, "A Hybrid PI-FOC and CCS-MPC Method for Multiple Harmonic Current Suppression in Multiphase Machines," in *2023 IEEE Int. Conf. Predictive Control Elect. Drives and Power Electron. (PRECEDE)*, 2023, pp. 1-7, doi: 10.1109/PRECEDE57319.2023.10174487.

[21] A. Choubey, P. K. Padhy and S. K. Jain, "Model Predictive Control for DC-DC Boost converter," in *2021 IEEE Conf. Energy Convers. (CENCON)*, 2021, pp. 58-63, doi: 10.1109/CENCON51869.2021.9627268.

[22] Y. Song, "Research on Control Strategy of Three-level PV Grid-Connected Inverter Based on FCS-MPC," in *2023 4th Int. Conf. Adv. Elect. and Energy Syst. (AEES)*, 2023, pp. 39-44, doi: 10.1109/AEES59800.2023.10468919.

[23] Y. Li, S. Sahoo, T. Dragičević, Y. Zhang, and F. Blaabjerg, "Stability-Oriented Design of Model Predictive Control for DC/DC Boost Converter," *IEEE Trans. Ind. Electron.*, vol. 71, no. 1, pp. 922-932, 2024, doi: 10.1109/TIE.2023.3247785.

[24] P. Karamanakos and T. Geyer, "Guidelines for the Design of Finite Control Set Model Predictive Controllers," *IEEE Trans. Power Electron.*, vol.35, no.7, pp.7434-7450, 2020, doi: 10.1109/TPEL.2019.2954357.

[25] M. S. Mousavi, S. A. Davari, V. Nekoukar, C. Garcia and J. Rodriguez, "A Robust Torque and Flux Prediction Model by a Modified Disturbance Rejection Method for Finite-Set Model-Predictive Control of Induction Motor," *IEEE Trans. on Power Electron.*, vol.36, no.8, pp.9322-9333, 2021, doi: 10.1109/TPEL.2021.3054242.

[26] X. Zhang, H. Zhang and K. Yan, "Hybrid Four-segment-mode Model Predictive Control for Open-winding PMSM Drives," *IEEE Transac. Transp. Electrific.*, vol. 10, no. 2, pp. 4322-4333, 2024, doi: 10.1109/TTE.2023.3308570.

[27] N. Guler, S. Biricik, S. Bayhan and H. Komurcugil, "Model Predictive Control of DC–DC SEPIC Converters With Autotuning Weighting Factor," *IEEE Trans Indus. Electron.*, vol. 68, no. 10, pp. 9433-9443, Oct. 2021, doi: 10.1109/TIE.2020.3026301.

[28] Y. Li, T. Dragičević, S. Sahoo, Y. Zhang, and F. Blaabjerg, "An Improved Model Predictive Control for DC-DC Boost Converter," in *2022 IEEE 13th Int. Symp. Power Electron. Distrib. Gener. Syst. (PEDG)*, 2022, pp. 1-6, doi: 10.1109/PEDG54999.2022.9923104.